Acta Crystallographica Section D
**Biological Crystallography**
ISSN 0907-4449

# Understanding the polymorphic behaviour of a mutant of the α-spectrin SH3 domain by means of two 1.1 Å resolution structures

**Ana Cámara-Artigas,[a]* Jose Antonio Gavira,[b] Salvador Casares,[c] Juan Manuel Garcia-Ruiz,[b] Francisco Conejero-Lara,[c] James P. Allen[d] and Jose C. Martinez[c]**

[a]Departamento de Química Física, Bioquímica y Química Inorgánica, Universidad de Almería, Spain, [b]Laboratorio de Estudios Cristalograficos–IACT (CSIC–Universidad de Granada), Spain, [c]Departamento de Química Física e Instituto de Biotecnología, Universidad de Granada, Spain, and [d]Department of Chemistry and Biochemistry, Arizona State University, USA

Correspondence e-mail: acamara@ual.es

Received 15 July 2010
Accepted 11 January 2011

SH3 domains are small protein modules that mediate the assembly of specific protein complexes, typically *via* binding to proline-rich sequences in their respective binding partners. Most of the α-spectrin SH3-domain (Spc-SH3) structures determined to date using X-ray diffraction have been solved from crystals belonging to the orthorhombic space group $P2_12_12_1$ with a needle-like morphology. All of these orthorhombic crystals exhibited a rapid growth rate. In addition to this crystal form, the R21D mutant of Spc-SH3 crystallizes in a new crystal form in the presence of sodium formate at pH values higher than 6. This new crystal form grows at a slower rate and belongs to the hexagonal space group $P6_522$, with unit-cell parameters $a = b = 42.9$, $c = 127.5$ Å. When both polymorphs of the R21D mutant of Spc-SH3 are simultaneously present into the same solution, it has been observed that the hexagonal crystals grow at the expense of the orthorhombic crystals. The availability of 1.1 Å resolution structures for both crystal forms allows the identification of key features that could account for the observed polymorphic behaviour.

## 1. Introduction

While polymorphic behaviour has been broadly studied in crystals of small molecules, few studies can be found in the literature concerning the molecular basis of the phenomenon in protein crystallization (Mangin *et al.*, 2009). In addition, one of the main criticisms of protein structures obtained by X-ray crystallography lies in the impact of the crystal contacts on the conformation of the protein. Therefore, the availability of different polymorphic crystals would permit the determination of the structures in different crystal environments and a study of the effect of the crystal contacts in a particular observed conformation. Consequently, a deeper knowledge of the origin of polymorphic behaviour in proteins would be helpful in their structural characterization.

The Src-homology region 3 (SH3) domain is a well characterized small protein module which is known to interact with proline-rich sequences. Its binding site is composed of a hydrophobic surface located between the RT and n-Src loops and three shallow pockets that are outlined by conserved aromatic residues. Two of the pockets accommodate the prolines in the P*xx*P motif and the third pocket, which is known as the 'specificity pocket', plays an important role in both the affinity and the specificity of the interaction (Cesareni, 2005).

One of the structurally best characterized SH3 domains is the chicken $\alpha$-spectrin SH3 domain (Spc-SH3). The first structure of Spc-SH3 was solved by Musacchio *et al.* (1992); since then, the structures of more than 20 different Spc-SH3 variants have been solved by means of X-ray and NMR (Vega *et al.*, 2000; Berisio *et al.*, 2001; Casares, Ab *et al.*, 2007; Casares, López-Mayorga *et al.*, 2007; Cámara-Artigas *et al.*, 2009). A common and interesting feature of crystals of Spc-SH3 is the very rapid growth that is observed when using ammonium sulfate or sodium formate as the precipitant agent. We have recently demonstrated that the origin of this behaviour is a specific interaction of the Pro20 residue located in the RT loop with the first pocket formed by residues Tyr13 and Tyr57 (Cámara-Artigas *et al.*, 2009). Furthermore, we have also shown that a lack of Pro20 not only delays crystal growth, but also changes the crystal space group from the orthorhombic $P2_12_12_1$ to the tetragonal $P4_12_12$. Next to the Pro20 residue, Arg21 also plays a crucial role in the protein-folding and binding properties of Spc-SH3. We have previously solved the structures of several other mutants at position 21 (Casares, López-Mayorga *et al.*, 2007) and all of the crystals obtained of single mutants at position 21 belonged to space group $P2_12_12_1$. The exception was the R21D mutant, which crystallized in two different space groups: the previously described orthorhombic space group and the hexagonal space group $P6_522$. Moreover, we have also observed that under certain experimental conditions the growth of the hexagonal crystals occurs at the cost of the orthorhombic crystals, which disappear at the same time following Ostwald's rule (Ostwald, 1897), which essentially describes the growth of the most thermodynamically stable form at the expense of the kinetically favoured form. Both crystal forms diffract to a resolution close to 1 Å and the availability of these high-resolution structures has allowed us to tackle the structural basis of the polymorphic behaviour of this protein.

## 2. Materials and methods

### 2.1. Protein purification

The R21D $\alpha$-spectrin SH3 mutant was overexpressed from a pET3d-type plasmid using the *Escherichia coli* BL21 (DE3) strain. The plasmid was a kind gift from Dr Luis Serrano (EMBL, Heidelberg). Cells were harvested by centrifugation and further lysed in 5.0 m*M* sodium citrate buffer pH 3.5 using a French press. The cell lysate was further acidified to pH 3.0 with diluted HCl, taking advantage of the high solubility of the protein at pH ∼3. Acidified cell lysate was clarified by ultracentrifugation and the protein was further recovered from the supernatant by precipitation in ammonium sulfate at 75% saturation. Precipitated protein was solubilized in 50.0 m*M* sodium phosphate buffer and 100 m*M* NaCl pH 7.0 containing 6.0 *M* urea and dialyzed extensively against the same buffer. The protein was then purified by a gel-filtration step on a HiLoad Superdex 75 column (GE Healthcare Life Sciences) and its purity was checked by SDS–PAGE. Protein aliquots were extensively dialyzed against pure water acidified to pH 3.0 with HCl and finally lyophilized for storage. For crystallization experiments, lyophilized protein was directly dissolved in 5.0 m*M* glycine pH 3.0 buffer and the concentration was determined spectrophotometrically as described previously (Casares, López-Mayorga *et al.*, 2007).

**Table 1**
Data-collection and refinement statistics for the R21D Spc-SH3 mutant structures.

Values in parentheses are for the highest resolution bin.

| Space group | $P2_12_12_1$ | $P6_522$ |
|---|---|---|
| pH | 6 | 6.5 |
| Temperature (K) | 100 | 298 |
| Precipitant | Ammonium sulfate | Sodium formate |
| Unit-cell parameters (Å) | $a$ = 34.8, $b$ = 42.2, $c$ = 48.4 | $a$ = 42.9, $b$ = 42.9, $c$ = 127.5 |
| Resolution range (Å) | 18–1.10 | 20–1.10 |
| No. of observations | 188031 | 119830 |
| Unique reflections | 28144 (2867) | 27903 (2330) |
| Data completeness (%) | 95.2 (98.8) | 99.8 (100) |
| $R_{\rm merge}$† (%) | 9.1 (30.2) | 7.5 (33.7) |
| $\langle I/\sigma(I)\rangle$ | 16.9 (6.4) | 16.8 (7.2) |
| Refinement | | |
| Protein residues | 58 | 58 |
| Solvent molecules | 110 | 43 |
| $R_{\rm work}$ (%) | 16.9 (24.1) | 15.7 (30.8) |
| $R_{\rm free}$ (%) | 19.2 (22.1) | 16.8 (31.8) |
| R.m.s. deviations from ideal geometry | | |
| Bonds (Å) | 0.019 | 0.022 |
| Angles (°) | 1.944 | 1.979 |
| Mean $B$ (protein) (Å$^2$) | 14.328 | 19.748 |
| Residues in allowed regions of the Ramachandran plot‡ (%) | 98 | 98 |

† $R_{\rm merge} = \sum_{hkl}\sum_i |I_i(hkl) - \langle I(hkl)\rangle| / \sum_{hkl}\sum_i I_i(hkl)$, where $I_i(hkl)$ is the intensity of an individual reflection and $\langle I(hkl)\rangle$ is the mean intensity of that reflection. ‡ From *PROCHECK* statistics.

### 2.2. Protein crystallization and data collection and analysis

Spc-SH3 crystallizes over a broad range of pH values using either ammonium sulfate or sodium formate. The presence of the hexagonal polymorph was initially observed in 2 *M* sodium formate, 0.1 *M* MES pH 6.5, the same conditions that were used to obtain optimized crystals of the orthorhombic crystal form. The presence of polymorphic behaviour was observed when either vapour-diffusion or batch-under-oil techniques were used to crystallize the protein. To characterize the formation of the polymorphs of the R21D mutant, several crystallization experiments were set up at 298 K. This temperature was chosen in order to avoid changes in temperature during crystal growth and observation.

To determine the optimum conditions for obtaining the hexagonal polymorph, several experiments were performed in Linbro plates and different protein and precipitant solution concentrations were tested. The experiments were therefore performed in a range of sodium formate concentrations between 1 and 6 *M* and of ammonium sulfate concentrations from 0.5 to 3 *M*. The pH-dependence was examined using 0.1 *M* buffers at pH values ranging from 4 to 9. The protein and precipitant solutions were mixed in a 1:1 ratio and 10 µl drops were equilibrated against 1000 µl precipitant solution in the reservoir. Owing to the nature of the precipitant solutions

with high concentrations of either sodium formate or ammonium sulfate, the final pH within the drop was carefully checked in each experiment. Some drift in the pH was observed and was therefore taken into account in the analysis of the experiments.

The high-resolution structure of the hexagonal polymorph was obtained from crystals grown in 2 *M* sodium formate and 0.1 *M* MES pH 6.5 and the structure of the orthorhombic polymorph was obtained from crystals grown in 0.8 *M* ammonium sulfate, 0.1 *M* bis-tris pH 6. Diffraction from both crystals was measured on BM16 at the European Synchrotron Radiation Facility (ESRF, Grenoble) using radiation of wavelength 0.97 Å. Data sets were indexed, integrated and scaled using the *HKL*-2000 suite. Table 1 summarizes the data-collection and refinement statistics.

To determine the solubility, four different protein concentrations (10, 7.5, 5 and 2.5 mg ml$^{-1}$) and six precipitant concentrations (1, 2, 3, 4, 5 and 6 *M* sodium formate) were tested in 0.1 *M* MES buffer pH 6.5. Protein drops (50 µl) were obtained by mixing the protein solution with the reservoir solution in a 1:1 ratio and this drop volume was finally equilibrated against 1000 µl reservoir solution. After one week, no further changes were observed and the drop solutions were centrifuged to measure the remaining protein concentration in the supernatant.

### 2.3. Structure resolution and refinement

The structures of the R21D Spc-SH3 mutant crystals were solved by molecular replacement using *MOLREP* (Vagin & Teplyakov, 2010). In both cases the asymmetric unit is composed of only one polypeptide chain, with Matthews coefficients of 2.0 Å$^3$ Da$^{-1}$ (51.8% solvent) and 2.3 Å$^3$ Da$^{-1}$ (49.4% solvent) for the orthorhombic and hexagonal crystal

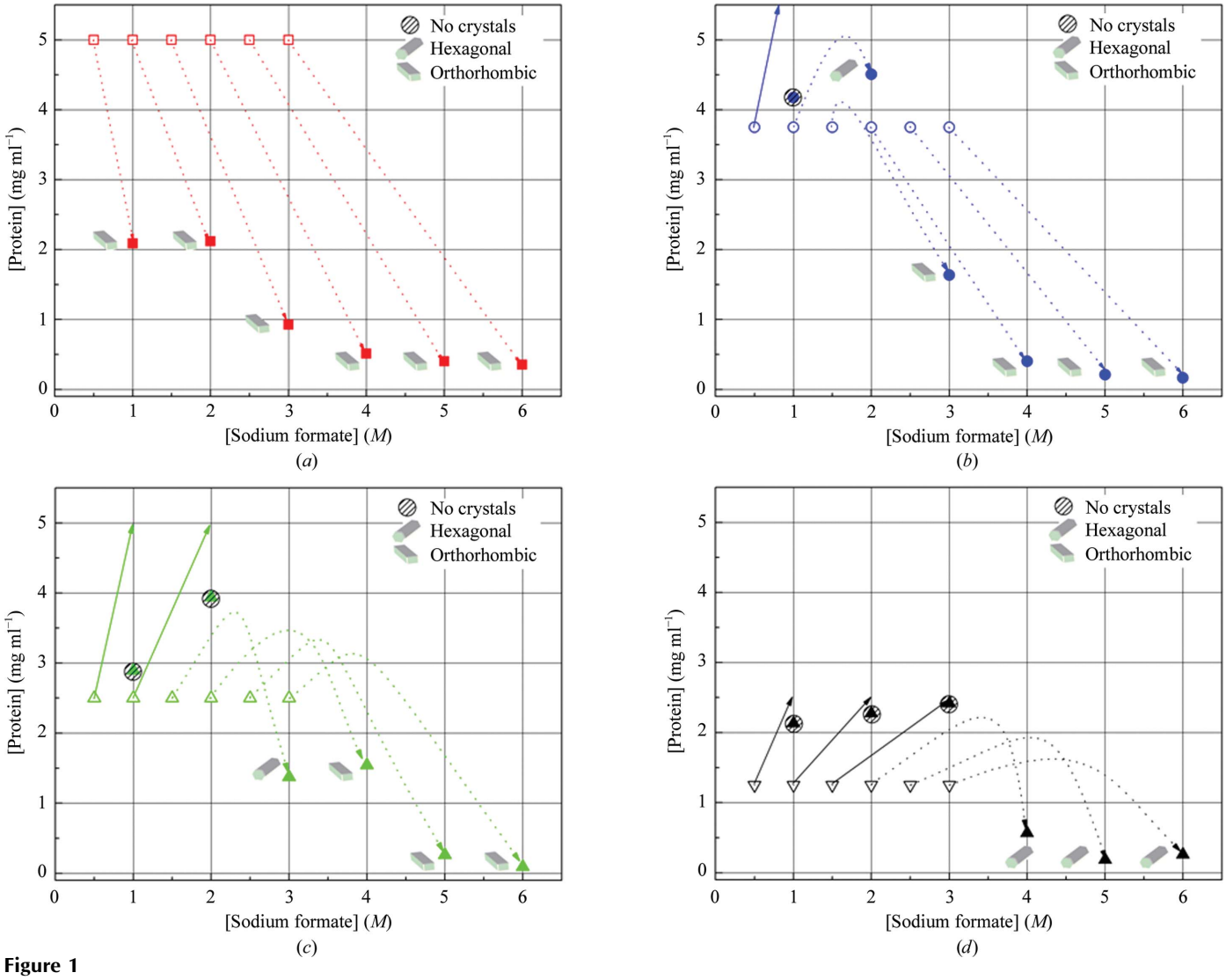


**Figure 1**
Protein concentration *versus* salt concentration plots showing initial concentration conditions (open symbols) for vapour-diffusion experiments at four different initial protein concentrations: (*a*) 5 mg ml$^{-1}$, (*b*) 3.75 mg ml$^{-1}$, (*c*) 2.5 mg ml$^{-1}$ and (*d*) 1.25 mg ml$^{-1}$. Drops were produced by mixing protein and precipitant solutions in a 1:1 ratio to give a final volume of 10 µl. The measured protein concentration after one week is shown by filled symbols. The changes in protein concentration over time are shown as arrows. Discontinuous arrows correspond to the hypothetical path giving rise to hexagonal or orthorhombic crystals, while continuous arrows indicate the final concentrations in drops with no crystal formation.

forms, respectively. The coordinates of wild-type Spc-SH3 (PDB code 1shg; Musacchio *et al.*, 1992) were used as a search model. The structures were refined using *REFMAC* v.5.0 (Murshudov *et al.*, 1997). Several cycles of positional refinement and temperature-factor refinement were alternated with manual building in the program *Coot* (Emsley & Cowtan, 2004) using $\sigma_A$-weighted ($2F_o - F_c$) and ($F_o - F_c$) electron-density maps. Water molecules were placed in the electron-density difference maps using *ARP*/*wARP* v.5.0 (Morris *et al.*, 2003) from the *CCP*4 suite (Collaborative Computational Project, Number 4, 1994). Superposition and calculation of the r.m.s.d. values of the structures were performed using the *CCP*4 program *LSQKAB* (Kabsch, 1976). A stereochemical analysis of the refined structures was performed with the program *PROCHECK* (Laskowski *et al.*, 1993). The final refinement statistics for the structure are presented in Table 1.

### 2.4. Crystal contact analysis

The protein interfaces in the crystals were characterized using the *PISA* server (Krissinel & Henrick, 2005) and the distances between amino acids were calculated using the program *CONTACT* from the *CCP*4 suite (Collaborative Computational Project, Number 4, 1994).

The protonation state of the ionizable residues involved in the salt bridges and the electrostatic potential surfaces were calculated with *APBS* (Baker *et al.*, 2001) *via* a *PyMOL* (DeLano, 2002) plug-in. Partial charges were assigned using the *PDB2PQR* server (Dolinsky *et al.*, 2007).

## 3. Results

### 3.1. Protein crystallization

The R21D mutant of Spc-SH3 crystallizes in two different crystal forms, $R21D_O$ and $R21D_H$, belonging to orthorhombic ($P2_12_12_1$) and hexagonal ($P6_522$) space groups, respectively. The $R21D_O$ polymorph appears over a broad range of pH values (4–9) and precipitant concentrations using ammonium sulfate (1–3 *M*) or sodium formate (2–6 *M*). The $R21D_H$ polymorph only appears under certain experimental conditions related to the protein concentration, the nature of the precipitant salt and the pH used to set up the crystallization experiments. Thus, the hexagonal polymorph was only observed when sodium formate was used as the precipitant and when the pH was higher than 6. Additionally, the hexagonal form only grows in a narrow range of precipitant and protein concentration values.

Fig. 1 shows diagrams in which protein concentration is plotted against precipitant concentration. This figure also shows the time evolution of the drops, considering the estimated time pathway of the drops across crystallization space (García-Ruiz, 2003). Briefly, the orthorhombic polymorph appears essentially instantaneously when a high concentration of both protein and precipitant is used, giving rise to a large number of very thin crystal needles that are stable for months. However, when the starting protein concentration is kept below 7.5 mg ml$^{-1}$ and the precipitant concentration ranges from 1 to 3 *M* sodium formate just a few needles appear together with a few hexagonal prisms, which develop within

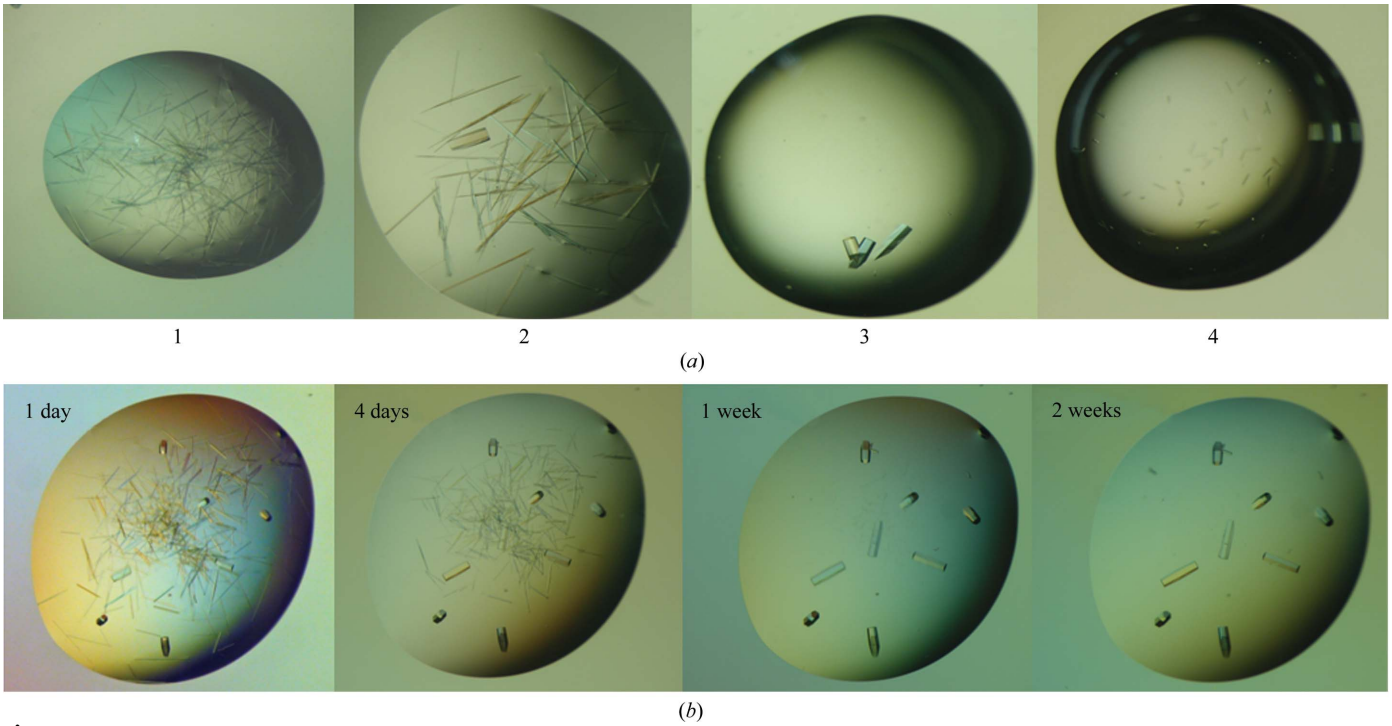


**Figure 2**
(*a*) Crystals grown under high (1), moderate (2, 3) and low (4) supersaturation conditions. (*b*) Evolution in time of a 10 µl drop with a starting protein concentration of 3.75 mg ml$^{-1}$ and 2 *M* sodium formate concentration. Just 1 d after setup of the experiment both $R21D_H$ and $R21D_O$ crystals grew simultaneously. Over time, the $R21D_O$ crystals dissolved back into solution in order to participate in the growth of the $R21D_H$ crystals. After two weeks, the only stable phase remaining in solution was the hexagonal one.

1–2 d (Fig. 2). At initial protein concentrations lower than 5 mg ml$^{-1}$ and precipitant concentrations ranging from 1 to 2 *M* no precipitation at all occurs during the experiment.

The most relevant result is that under the specific experimental conditions in which long needles and hexagonal prisms simultaneously develop in the drop, the hexagonal crystal form grows at the expense of the orthorhombic crystal from and within a few weeks the hexagonal crystal form is the only form remaining in the drop (Fig. 2). This result clearly indicates that whereas the R21D$_O$ is the kinetically favoured polymorph, the R21D$_H$ polymorph is thermodynamically favoured.

### 3.2. Spc-SH3 R21D mutant structures

The orthorhombic and hexagonal structures both show the same overall fold found in previous Spc-SH3 structures. Apart from some differences at the C- and N-termini, only subtle changes are found within the loops connecting strands $\beta$1–$\beta$2 (RT loop), $\beta$3–$\beta$4 (n-Src loop) and $\beta$5–$\beta$6 (distal loop). Indeed, both structures show only one residue that is outside the most favoured regions of the Ramachandran plot: Asn47 within the distal $\beta$-turn formed by residues Val46-Asn47-Asp48-Arg49. This residue is also outside the most favoured regions of the Ramachandran plot in all previously reported Spc-SH3 structures (Vega *et al.*, 2000). The differences found in the distal loop can also be explained by the different participation of this loop in the crystal packing of the two crystal forms and the poor electron density available to model the loop, which is reflected in the high *B*-factor values found in the structures of both polymorphs.

As expected, the major coordinate differences in the backbone of the two structures are located in the RT loop formed by residues Ser19, Pro20, Arg21 and Glu22. These differences are larger than those found between the different crystal structures of other R21 mutants (R21A and R21G; PDB entries 2f2w and 2f2x, respectively; Casares, López-Mayorga *et al.*, 2007) and wild-type Spc-SH3. All of these structures were solved in space group $P2_12_12_1$; moreover, we have previously shown that residue Pro20 is crucial in crystal packing in the orthorhombic crystal form (Cámara-Artigas *et al.*, 2009). Thus, it seems that the main backbone deviations between crystal forms arise from an RT-loop rearrangement that allows crystal contacts in each crystal form.

### 3.3. Protein contacts

To rationalize the molecular origin of the polymorphic behaviour of the R21D mutant, it is important to determine which residues are involved in contacts in each crystal form. With this purpose, we analyzed the protein interfaces using the *PISA* web server (Krissinel & Henrick, 2005). The details of each interface for each polymorph are compiled in Fig. 3, in which the packing of the asymmetric unit for each crystal form is shown (Fig. 3*a*). The R21D$_O$ and R21D$_H$ crystal forms share the first interface and the contacts present in both of them are identical (Fig. 3*b*), with ASA values upon interface formation of 449 and 481 Å$^2$, respectively. The differences arise when we compare the second interface (Fig. 3*c*). In the R21D$_O$ structure this interface is characterized by the burial of the Pro20 residue and a hydrophobic pocket formed by Tyr13 and Tyr57. However, in the R21D$_H$ structure the second interface shows interactions between the same aromatic residues and residue Lys18 instead of Pro20.

The hexagonal crystal form is characterized by the presence of a third interface, in which a formate molecule can be modelled bridging two Lys59 residues from symmetry-related molecules (Fig. 4*a*). This contact allows the placement of the Lys59 residue of the symmetry-related molecule on this third interface at a distance of 5.9 Å from residue Asp21. In the orthorhombic crystal form this interface is not present and a sulfate ion has been modelled between Lys59 and Lys60 (Fig. 4*b*). In R21D$_O$ neither the ion nor Lys59 participate in crystal contacts. In order to evaluate the role of electrostatic interactions in the packing of each crystal cell, the electrostatic surfaces were calculated using the program *APBS* (Baker *et al.*, 2001). The electrostatic surface of each crystal form and the most salient contacts are shown in Fig. 4.

## 4. Discussion

To clarify the polymorphic behaviour of the R21D mutant of Spc-SH3, the structures of the orthorhombic and hexagonal crystals have been solved at a resolution of 1.1 Å. The new hexagonal crystal form of the R21D mutant belonged to space group $P6_522$ and only appeared under conditions in which the orthorhombic crystals nucleate and grow at sufficiently slow rates to give time for the hexagonal crystal form to nucleate before the protein concentration is greatly depleted. Multiple crystallization experiments conducted at several protein and precipitant concentrations, as well as at different pH values ranging from 4 to 9, indicate that at high supersaturation values the very rapid nucleation and growth of the orthorhombic crystals reduces the supersaturation level quickly. Therefore, the protein concentration becomes so low that it prevents nucleation of the hexagonal crystal form. However, under moderate supersaturation conditions both crystal forms can nucleate and coexist in the same solution and the growth of the hexagonal crystals takes place at the expense of the orthorhombic crystals (Fig. 2). This behaviour is in full agreement with Ostwald's rule (Ostwald, 1897); in our system the slow-growing thermodynamically favoured crystal form (R21D$_H$) grows at the expense of the fast-growing kinetically favoured form (R21D$_O$).

We have also analyzed the contacts established within the crystal cell of each polymorph in order to understand the origin of the distinct behaviour observed in their crystallization. Analysis of the protein interfaces reveals that the orthorhombic and hexagonal crystal forms share the same first interface (Figs. 3*a* and 3*b*). This first interface is also shared by a tetragonal crystal form obtained using a triple mutant of Spc-SH3 (Cámara-Artigas *et al.*, 2009). In addition, the presence of the same dimeric species forming the first interface of the hexagonal crystal form is indicative of the fact that the crystallization mechanism previously proposed for the

orthorhombic and tetragonal crystal forms also applies to the hexagonal crystal form (Cámara-Artigas *et al.*, 2009).

As the first interface does not show significant differences between crystal forms, we hypothesize that the differences in thermodynamic stability and kinetic behaviour that we observe between crystal forms might relate to the second interface. The second interface of the hexagonal crystal form is formed by interactions between residues Lys18 and Tyr13–Tyr57 of symmetry-related molecules. Therefore, the lower growth rate that we observe for the R21D$_{H}$ form can be attributed to the absence of the Pro20–Tyr13–Tyr57 contact within the protein crystal. As described previously (Cámara-Artigas *et al.*, 2009), the presence of this contact in the second interface of the orthorhombic crystal form of Spc-SH3 may explain the unusually rapid growth rate of these crystals. Accordingly, at high protein and precipitant concentrations only the formation of the orthorhombic polymorph is observed, since this is the form favoured by the specific contact between Pro20 and the symmetry-related couple Tyr13–Tyr57.

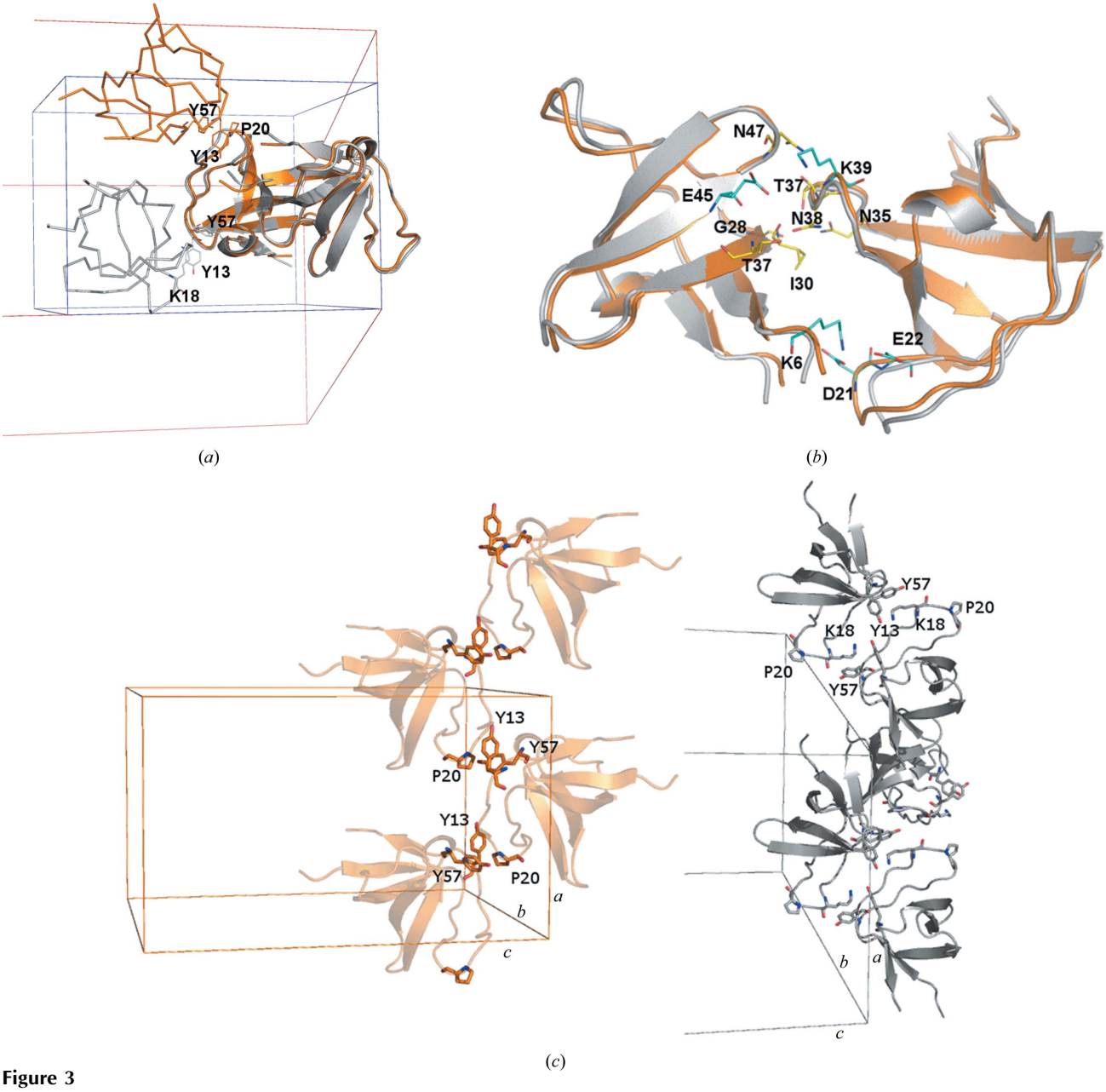


**Figure 3**
(*a*) The first interface of the orthorhombic (orange) and hexagonal (grey) crystal forms of the R21D mutant of Spc-SH3 is shown as a thick ribbon cartoon. The second interface of each crystal form is shown as a thin ribbon cartoon. Critical residues in the contact of the second interface are shown in stick representation. Both crystal forms have been superposed taking the dimer present in both crystal forms as a reference. (*b*) Detail of the first interface of the orthorhombic (orange) and hexagonal (grey) crystal structures. Residues involved in hydrogen bonds are shown as yellow sticks and those involved in salt bridges are shown as cyan sticks. (*c*) Detail of the second interface of the orthorhombic (orange) and hexagonal (grey) crystal forms. Residues forming the contact at the second interface are shown as sticks. This contact propagates along the *a* axis of each crystal cell.

However, at low protein and precipitant concentrations the growth rate is sufficiently slowed to allow nucleation of the hexagonal polymorph. Thus, when both crystal forms develop within the same solution the hexagonal crystals grow at the expense of the orthorhombic crystals. This behaviour is indicative of a higher thermodynamic stability of the hexagonal crystal form under the experimental conditions tested, where both crystal forms coexist. We have found that this situation only occurs under restricted conditions of pH and precipitating agent. In this way, the structure of the R21D mutant has been solved over a broad range of pH values (4–9) in the presence of two precipitants: ammonium sulfate and sodium formate. The orthorhombic crystal form is the only one that appears in the presence of ammonium sulfate at all pH values, whereas the hexagonal polymorph only appears in the presence of sodium formate at pH values higher than 6. Similarly, the failure to crystallize the hexagonal polymorph at pH values lower than 6 suggests that some acidic unprotonated residues may play key roles in the stability of the hexagonal crystal form. Additionally, we have previously solved the structures of several Spc-SH3 variants with mutations at the Arg21 position (Casares, López-Mayorga *et al.*, 2007) and all of them crystallize in the orthorhombic space group $P2_12_12_1$ with essentially the same crystal cell. The new hexagonal crystal form has only been observed when the arginine is replaced by aspartate, which indicates a crucial role for Asp21 in the stabilization of this crystal form.

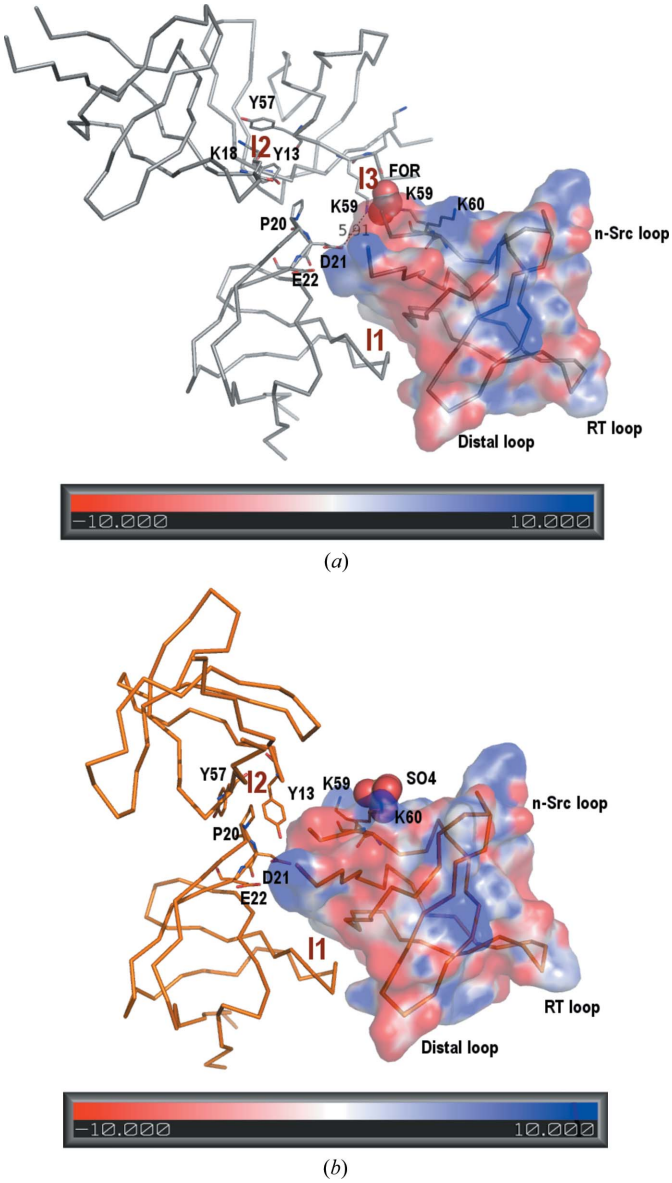


**Figure 4**
Electrostatic surface of (*a*) the hexagonal (grey) and (*b*) the orthorhombic (orange) crystal forms. Details of the relevant residues in the contacts are shown. The interfaces of each crystal form are also indicated. The precipitant molecules modelled in each crystal form and their respective contact residues are also shown. A formate ion (FOR) is located between the Lys59 residues of two symmetry-related molecules in the third interface of the hexagonal crystal form, while a sulfate ion (SO4) is found between Lys59 and Lys60.

To evaluate the effect of the negative charge of Asp21 on the stability of the crystal form, the electrostatic surface of the domain has been calculated using *APBS* for each crystal form. The most relevant difference found between the polymorphs is evident in the electrostatic interactions in the third interface of the hexagonal crystal form (Fig. 4*a*). In this interface the Lys59 residue of the third SH3-domain molecule is placed at a distance of 5.9 Å from Asp21. The electrostatic interaction between the opposite charged aspartate and lysine residues would be favoured if the aspartate is unprotonated, which might explain the pH-dependence of the hexagonal polymorph formation.

We note the presence of a formate molecule interacting with two Lys59 residues of symmetry-related molecules in the third interface of the hexagonal crystal form (Fig. 4*a*). The presence of the formate ion could play a key role in the interaction that facilitates the crystal contact along the hexagonal screw axis. Many polymorphic protein crystals have been obtained by modification of the precipitant solution, but the molecular basis has not been studied deeply. One of the most important limitations to carrying out these studies is the inherent difficulty in modelling precipitant molecules. In recent years, the availability of a growing number of high-resolution structures has fortunately changed this situation. Consequently, the high resolution of our R21D mutant structures allows us to model some precipitant molecules together with the crystal forms obtained either in ammonium sulfate or sodium formate. In the case of $R21D_O$ a sulfate ion has been modelled between the Lys59 and Lys60 residues at a distance of ∼5 Å from the NZ group of each lysine residue (Fig. 4*b*). The presence of this sulfate ion could exert a strong shielding effect that prevents interaction between the Lys59 residues of symmetry-related molecules and subsequently prevents nucleation of this polymorph. In fact, in this crystal form neither Lys59 nor Lys60 participate in crystal contacts.

The best studied of the polymorphic protein crystals described in the bibliography are those of porcine pancreatic α-amylase (Boistelle *et al.*, 1992) and bovine pancreatic trypsin inhibitor (BPTI; Hamiaux *et al.*, 2000). In both cases, the thermodynamic and kinetic parameters governing the formation of the different polymorphic crystal forms have been

reported (Astier & Veesler, 2008). Interestingly, BPTI shows a similar behaviour to that of R21D: the space group depends on the salt used to crystallize the protein and the presence of prenucleation aggregates in solution has also been reported. In the case of BPTI, crystal growth takes place by stacking of BPTI decamers in the resulting crystal, but the effect of different salts on the resulting space group has not been described. In our case, the availability of high-resolution structures of R21D Spc-SH3 has allowed us to model key molecules from the precipitant solution which may account for the polymorphic behaviour observed in this mutant of Spc-SH3. This information is extremely helpful since it can help in understanding the molecular basis of polymorphic behaviour in proteins.

This research was funded by grants BIO2006-15517-C02-01/02 and BIO2009-13261-C02-01/02 from the Spanish Ministry of Education and Sciences, and grants CVI-05063 and CVI-05915 from the BIO-328 and FQM-171 research group of the Andalusian Regional Government. We would also like to thank the OptiCryst project of the Sixth Framework of the EU and the 'Factoría Española de Cristalización' Ingenio/Consolider 2010 and Professor Jose-Carlos Redondo-Olmedilla for revising the English text.

## References

Astier, J.-P. & Veesler, S. (2008). *Cryst. Growth Des.* **8**, 4215–4219.
Baker, N. A., Sept, D., Joseph, S., Holst, M. J. & McCammon, J. A. (2001). *Proc. Natl Acad. Sci. USA*, **98**, 10037–10041.
Berisio, R., Viguera, A., Serrano, L. & Wilmanns, M. (2001). *Acta Cryst.* D**57**, 337–340.
Boistelle, R., Astier, J.-P., Marchis-Mouren, G., Desseaux, V. & Haser, R. (1992). *J. Cryst. Growth*, **123**, 109–120.
Cámara-Artigas, A., Andújar-Sánchez, M., Ortiz-Salmerón, E., Cuadri, C. & Casares, S. (2009). *Acta Cryst.* D**65**, 1247–1252.
Casares, S., Ab, E., Eshuis, H., Lopez-Mayorga, O., van Nuland, N. A. & Conejero-Lara, F. (2007). *BMC Struct. Biol.* **7**, 22.
Casares, S., López-Mayorga, O., Vega, M. C., Cámara-Artigas, A. & Conejero-Lara, F. (2007). *Proteins*, **67**, 531–547.
Cesareni, G. (2005). *Modular Protein Domains.* Weinheim: Wiley-VCH.
Collaborative Computational Project, Number 4 (1994). *Acta Cryst.* D**50**, 760–763.
DeLano, W. L. (2002). *PyMOL.* http://www.pymol.org.
Dolinsky, T. J., Czodrowski, P., Li, H., Nielsen, J. E., Jensen, J. H., Klebe, G. & Baker, N. A. (2007). *Nucleic Acids Res.* **35**, W522–W525.
Emsley, P. & Cowtan, K. (2004). *Acta Cryst.* D**60**, 2126–2132.
García-Ruiz, J. M. (2003). *Methods Enzymol.* **368**, 130–154.
Hamiaux, C., Pérez, J., Prangé, T., Veesler, S., Riès-Kautt, M. & Vachette, P. (2000). *J. Mol. Biol.* **297**, 697–712.
Kabsch, W. (1976). *Acta Cryst.* A**32**, 922–923.
Krissinel, E. & Henrick, K. (2005). *CompLife* 2005, edited by M. R. Berthold, R. Glen, K. Diederichs, O. Kohlbacher & I. Fischer, pp. 163–174. Berlin, Heidelberg: Springer-Verlag.
Laskowski, R. A., MacArthur, M. W., Moss, D. S. & Thornton, J. M. (1993). *J. Appl. Cryst.* **26**, 283–291.
Mangin, D., Puel, F. & Veesler, S. (2009). *Org. Process Res. Dev.* **13**, 1241–1253.
Morris, R. J., Perrakis, A. & Lamzin, V. S. (2003). *Methods Enzymol.* **374**, 229–244.
Murshudov, G. N., Vagin, A. A. & Dodson, E. J. (1997). *Acta Cryst.* D**53**, 240–255.
Musacchio, A., Noble, M., Pauptit, R., Wierenga, R. & Saraste, M. (1992). *Nature (London)*, **359**, 851–855.
Ostwald, W. (1897). *Z. Phys. Chem.* **22**, 289–330.
Vagin, A. & Teplyakov, A. (2010). *Acta Cryst.* D**66**, 22–25.
Vega, M. C., Martínez, J. C. & Serrano, L. (2000). *Protein Sci.* **9**, 2322–2328.